Theor Chem Account (2008) 120:263–271
DOI 10.1007/s00214-007-0301-y

REGULAR ARTICLE

Theoretical study of environmental effects on proton transfer reaction through the peptide bond in a model system

Toshio Asada · Tadayoshi Takahashi · Shiro Koseki

Received: 20 November 2006 / Accepted: 16 February 2007 / Published online: 15 May 2007

Abstract This study considered the possibility of proton transfer reactions through the peptide bond under different environments using the dipeptide and the 12-mer polyglycine α-helix models, in which diglycine is substituted by the 12-mer polyglycine helix. Ab initio molecular orbital calculations were carried out at the B3LYP/6-31+G(d) level of theory. To evaluate the free energies in solution, calculations of the solvation energies were performed using PCM. The correction functions on the calculated solvation energies were provided to reproduce experimental pKa values. The proton transfer reactions through the peptide bond are concluded to be possible in the protein for a wide range of proton acceptors. His complex has two free energy minima along a putative proton transfer pathway in spite of one minimum in the other complexes. The α-helix is estimated to suppress the proton transfer reactions through the peptide bond at the termini of the helix, although it is possible to proceed when the proton affinity of the acceptor is low.

Keywords Proton transfer reaction · Peptide bond · Solvation free energy · Alpha helix · Environmental effect

1 Introduction

Proton transfer reactions are highly significant fundamental chemical events in the gas phase [1–7], in solvents [8,9], and also in biological systems [10,11]. Recently, Tsukihara et al. experimentally investigated the proton pumping process in cytochrome c oxidase [11], and suggested that proton transfer through peptide bonds is possible. When a proton is added to a peptide carbonyl group, an imidic acid [–C(OH) $= N^+H$–] is formed. If a proton-accepting group is located near the $= N^+H$– moiety, it will extract a proton to produce the enol form of the peptide [–C(OH)=N–]. However, there have been only a few theoretical investigations [10] on this type of proton transfer reactions in proteins. Therefore, we have systematically studied the possibility of proton transfer reactions and also investigated the environmental effects on this type of reaction from a theoretical point of view.

In general, the consideration of the environmental effects is very important in order to describe the exact potential energy surface under various circumstances. As the general consensus, the acidity and basicity, which are concerned with the proton transfer events, of small molecules in the gas phase can be calculated as well as or even better than it can be measured. The situation is less satisfactory in solution due to the difficulty of quantitatively calculating the solvation energies with good accuracy. Nevertheless, it is clear that the dielectric continuum models have been most popular to estimate the solvation free energies, because of their unique combination of simplicity, utility and efficiency. For the purpose of obtaining qualitative information on proton transfer reactions in water and also in proteins, we have considered the environmental effects on the reaction energy and energy barrier of a reaction in calculating the solvation free energies by applying the polarizable continuum model (PCM) [12], which offers an economic and efficient calculation of solvation free energies.

Besides the solvation effects, the secondary structures play an important role in the stability of the system in proteins. Hole reported that in proteins, the helix macrodipole is implicated in the function and stabilizing structural motifs

Contribution to the Mark S. Gordon 65th Birthday Festschrift Issue.

T. Asada (✉) · T. Takahashi · S. Koseki
Department of Chemistry, Faculty of Science,
Osaka Prefecture University, 1-1 Gakuen-cho, Naka-ku, Sakai,
Osaka 599-8531, Japan
e-mail: asada@c.s.osakafu-u.ac.jp

containing helix pairs [13,14]. Furthermore, the helix dipole moment has been suggested to influence the pKa values [15] and to stabilize the presence of charged residues at the helix termini [16]. Recently, Sek et al. experimentally demonstrated that the electron transfer through an α-helical peptide is very efficient, and there is a directional dependence of electron transmission through the peptide, which is connected to the electric field generated by the molecular dipole of the helix [17]. Sengupta et al. reported the effects of the helix environment in screening and modulating the helix dipole [18]. They have suggested that the helix dipole is relatively strong in the protein environment, which is about 15–20 Debye for the 12-mer polyalanine α-helix.

We report the stable structures and energies of intermediates along the proton transfer pathway using the simple diglycine model and the 12-mer polyglycine α-helix determined by ab initio molecular orbital calculations. The stability of intermediates will be accounted for with respect to the proton affinities (PAs) and the pKa values of proton-accepting amino acids located near the NH moiety of the peptide bond. The PA of acceptors significantly affect the shape of the potential energy surfaces along the proton transfer pathway. In proteins, a proton transfer reaction is possible for a wide range of proton acceptors; however, it becomes difficult to proceed in water. The α-helix suppresses proton transfer reactions at the terminal of the α-helix, although it is possible to proceed when the PA of the acceptor is low, in contrast to the reported efficiency of the electron transfer reactions through the peptide. On the basis of calculated results, a systematic discussion of the possibility of proton transfer reactions and the effects of the dipole moment on this reaction are presented.

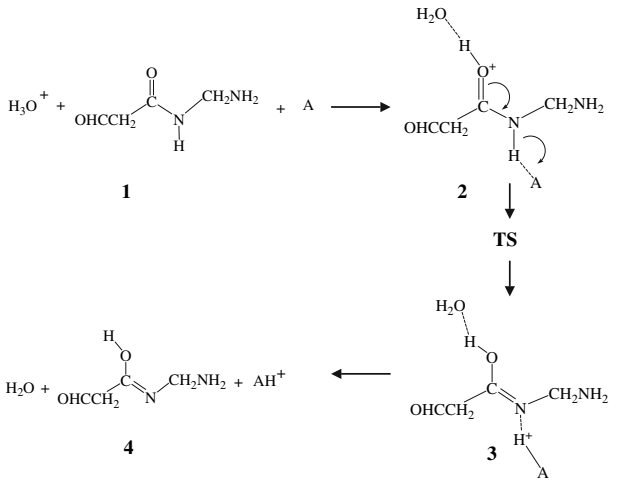

Fig. 1 Schematic representation of proton transfer pathway in the model diglycine

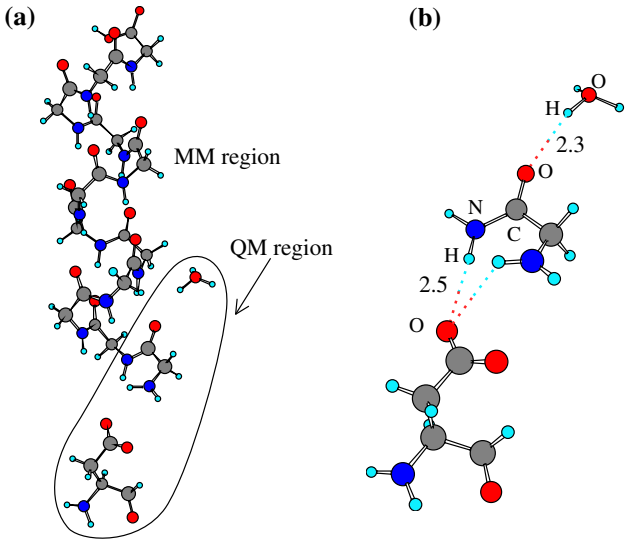

Fig. 2 a-helix model compound. **a** QM/MM division in the 12-mer polyglycine complex, **b** hydrogen atom capped QM structure (bond lengths in Å)

2 Method

2.1 Model structure setting

Figure 1 shows a schematic representation of the proton transfer pathway in the diglycine model, in which keto-enol tautomerization can be seen. Compound **1** consists of the isolated model diglycine, oxonium ion and the given proton acceptors with no intermolecular interactions, in which the proton acceptor is one of the different kinds of amino acids with a variety of acid strengths and the peptide bond has the stable keto form. Complex **2** is a reaction intermediate, which is obtained by proton transfer from the oxonium ion to the carbonyl oxygen in a peptide bond. The proton in the N–H bond then transfers to an acceptor to form complex **3**. Compound **4** is the isolated molecules that consist of water, the enol-type isomer of diglycine and a protonated proton acceptor. We have used model aspartic acid anion (Asp^-), glutamic acid anion (Glu^-), histidine (His), arginine (Arg) and water molecules as the proton acceptors to elucidate the free energy profiles depending on a wide range of acidities of the proton acceptor, in which the experimental pKa for Asp^-, Glu^-, His, Arg and water are 3.3, 4.1, 6.8, 12.5 and 15.7, respectively[19–21]. The second model is the α-helix model compounds shown in Fig. 2, in which the reaction site is located at the N-terminal residue in the α-helix that consists of the 12-mer polyglycine. The model α-helix is provided by substituting all the component residues with glycine in the α-helix of the enzyme (PDB code 1V54), ranging from His12 to Gly23, and then a proton donor and a proton acceptor are coordinated of the appropriate positions as seen in Fig. 2.

Table 1 Calculated proton affinities compared with experimental values (in kcal/mol)

Acid/Base	Proton affinity[a]	Exp
H_3O^+/H_2O	168.8	170.0[b]
Hdiglycine$^+$/diglycine(enol)	237.6	
HHis$^+$/His	243.6	236.0[c]
HArg$^+$/Arg	253.3	251.2[d]
Asp/Asp$^-$	337.4	
Glu/Glu$^-$	339.9	

[a] Proton affinity is given by the difference of the total electronic energy between the acid and the base
[b] Ref. 23
[c] Ref. 24
[d] Ref. 25

2.2 Ab initio MO calculations and solvation free energy calculations

All the geometry optimizations were performed using the Gaussian03 program [22]. Normal-mode analyses were carried out to verify that the optimized structures are either true minima or transition states on the potential-energy surface and to obtain the entropy of the molecule. In the present paper, the B3LYP calculations using 6-31+G(d) basis set were applied to obtain the electronic energies because the system sizes are large. Table 1 lists the comparison between the calculated PAs and the experimental values [23–25]. The calculated PA of 168.8 kcal/mol for water and 253.3 kcal/mol for Arg are in reasonable agreement with the measured one of 170.0 and 251.2 kcal/mol, respectively. Rak et al. [26] used the high level ab initio MO method to obtain the PA of Arg to be 256.3 kcal/mol using the CCSD/6-311++G(d,p) level of theory. Although the deviation from the experimental value for His is relatively high, calculated PA can provide a valid qualitative tendency of the experimental PA. Thus, we consider that the B3LYP/6-31+G(d) level of theory is appropriate for the purpose in the present research.

To elucidate the reaction in the solvent, the hydration free energies were calculated using PCM with a Merz–Kollman cavity. Under the thermodynamic cycle 1, the free energy change from the compound **A** to **B** in a solvent, $\Delta G^{\mathbf{A}\to\mathbf{B}}_{\text{solvent}}$, can be written as

$$\Delta G^{\mathbf{A}\to\mathbf{B}}_{\text{solvent}} = \Delta G^{\mathbf{A}\to\mathbf{B}}_{\text{gas}} + \Delta\Delta G^{\mathbf{A}\to\mathbf{B}}_{\text{s}} \tag{1}$$

where,

$$\Delta\Delta G^{\mathbf{A}\to\mathbf{B}}_{\text{s}} = \Delta G^{B}_{\text{s}} - \Delta G^{A}_{\text{s}}. \tag{2}$$

$\Delta G^{\mathbf{A}\to\mathbf{B}}_{\text{gas}}$ and ΔG^{i}_{s} denote the free energy change in the gas phase and the solvation free energy of the solute i, respectively. The free energy change in the gas phase can be expanded as

$$\Delta G^{\mathbf{A}\to\mathbf{B}}_{\text{gas}} = \Delta H^{\mathbf{A}\to\mathbf{B}} - T\Delta S \tag{3}$$

where

$$\Delta H^{\mathbf{A}\to\mathbf{B}} = \Delta E^{\mathbf{A}\to\mathbf{B}} + \Delta ZPE^{\mathbf{A}\to\mathbf{B}} + P\Delta V. \tag{4}$$

H is the zero point energy corrected enthalpy, T is the absolute temperature, S is the entropy of the solute, E is the electronic energy, ZPE is the zero point energy, P is the pressure and V means the volume.

2.3 QM/MM calculations

The QM/MM techniques that combine quantum mechanics (QM) for the reactive region and molecular mechanics (MM) for the remainder are applied to optimize the α-helix model complexes. The QM/MM division splits the systems along a chemical bond. Therefore, we need to cap the QM subsystem with the so-called link atom. This link atom is presented as a hydrogen atom in the QM calculation step. The QM subsystem, in which proton transfer proceeds, is calculated using the Gaussian03 package, and the MM region and QM/MM interaction energies are estimated by our original code, in which the Amber99 force fields [27] are used to evaluate the MM energies. The electrostatic interactions between the QM and the MM regions are simultaneously solved in MO calculation steps. The QM/MM division is illustrated in Fig. 2.

3 Results and discussion

3.1 Diglycine model

3.1.1 Structures and energies

Figure 3 shows the optimized structures and some interatomic distances obtained by ab initio MO calculations. In all the structures, the hydroxyl and NH_2 terminal groups in diglycine are bridged by the water molecule. Complex **3** is the only available structure (Figs. 3a, b) for Asp$^-$ and Glu$^-$, whereas two complexes **2** and **3** are found for His and Arg. Thus, the transition states **TS** between these two complexes are addressed and shown in Figs. 3d and g, which have a linear arrangement proton bound N1$\cdots$H2$\cdots$N2 form. Comparing the positions of the bounded H2 atom in **TS**, the shorter bond length R(N1–H2) of 1.21 Å is observed in the Arg complex, which is regarded as the early transition state. The most likely reason is that the high PA of a proton acceptor lowers the energy of complex **3**; thus it takes an early transition state and the activation energy becomes low. If PA of the acceptor is significantly high, such as in Asp$^-$ and Glu$^-$, the **TS** are no longer present. We can compare the PA between the protonated Hdiglycine$^+$ and acceptors. Table 1 shows that the PAs of Asp$^-$ and Glu$^-$ are 337.4 and 339.9 kcal/mol,

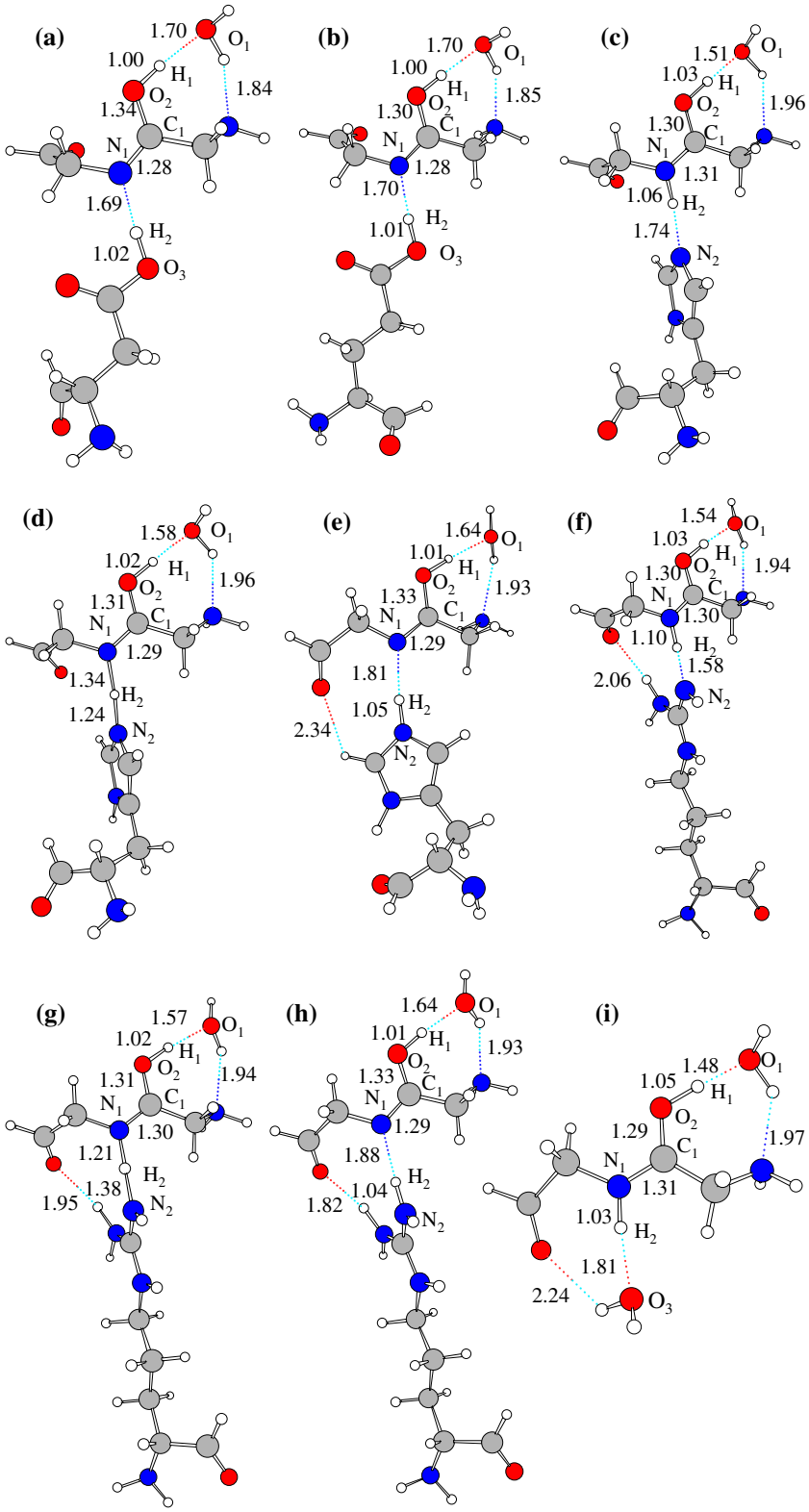

Fig. 3 Optimized structures (bond lengths in Å). **a** Asp^- complex **3**, **b** Glu^- complex **3**, **c** His complex **2**, **d** His TS, **e** His complex **3**, **f** Arg complex **2**, **g** Arg TS, **h** Arg complex **3**, **i** H_2O complex **2**

respectively, in spite of 237.6 kcal/mol for diglycine. Therefore, the energy barrier disappeared due to large difference in the PA of ca. 100 kcal/mol. On the other hand, the transition state **TS** is observed for His and Arg, since the PAs are comparable to that of diglycine. Based on this meaning, it is reasonable that complex **2** is the only available structure in the water complex, where the PA of water is 68.8 kcal/mol smaller than that of diglycine.

Table 2 lists the calculated thermodynamic properties on the enthalpy difference relative to complex **1**. Impressive

Table 2 Calculated thermodynamic properties contributing to the enthalpy difference relative to the compound **1**

	B	Electronic Energy (hartree)	$\Delta E^{1\to B}$ (kcal/mol)	$\Delta ZPE^{1\to B}$ (kcal/mol)	$\Delta H^{1\to B}$ (kcal/mol)
H_2O	**1**	−570.31939	0.0	0.0	0.0
	2	−570.45146	−82.9	4.6	−79.5
	4	−570.29681	14.2	0.0	14.2
Asp^-	**1**	−930.43731	0.0	0.0	0.0
	3	−930.72002	−177.4	3.9	−174.7
	4	−930.68344	−154.5	0.2	−154.3
Glu^-	**1**	−969.74570	0.0	0.0	0.0
	3	−970.02952	−178.1	3.7	−175.6
	4	−969.99578	−156.9	0.1	−156.8
His	**1**	−967.42566	0.0	0.0	0.0
	2	−967.56633	−88.3	3.3	−86.2
	TS	−967.55968	−84.1	0.6	−84.7
	3	−967.57885	−96.1	4.1	−93.3
	4	−967.52231	−60.6	0.8	−59.9
Arg	**1**	−1025.19657	0.0	0.0	0.0
	2	−1025.34652	−94.1	2.7	−92.6
	TS	−1025.34543	−93.4	0.9	−93.8
	3	−1025.35660	−100.4	3.4	−98.3
	4	−1025.29803	−63.7	−0.5	−64.1

stabilizations can be seen for the reaction from compound **1** to complex **3** for all proton acceptors except for H_2O. These stabilizations mainly come from the protonation energies of the acceptors in complex **3**, which compensates for the destabilization energies of the proton release from the oxonium ion. The electronic energy shows that complex **2** is less stable than complex **3** by 7.8 and 6.3 kcal/mol for His and Arg, respectively. The activation barrier to generate complex **3** from complex **2** for His and Arg are 4.2 and only 0.7 kcal/mol, respectively. The small barrier in the Arg complex will disappear by taking the ZPE corrections, and then complex **3** becomes the only available complex. In summary, once the oxonium ion coordinates to the peptide C=O bond, the N–H proton immediately transfers to a proton acceptor to make complex **3** with no enthalpy barriers for the Asp^-, Glu^-, and Arg complexes; nevertheless, there are two stable structures, which are separated by a transition state, for the His complex.

3.1.2 Free energy analysis

Whereas the enthalpy changes are the most important thermodynamic properties for the relative stability of the systems in the vacuum state, it does not hold true in the solvent, and the solvent effects significantly affect the stability of the solutes, especially in the solvent, represented by the high relative dielectric constant such as in water. In view of the scarcity of information on the proton transfer reaction in solution, we have considered the solvent effect on the reaction energy and energy barrier of the reaction by calculating the hydration free energies of the reactants, products and transition state structure.

Table 3 summarizes the calculated thermodynamic properties concerning pKa values of the proton acceptors used in this paper by applying the PCM method. In general, the solvation free energy changes ΔG_s^i or the absolute pKa values are difficult to accurately calculate. Chipman et al. [28] have reported the calculated pKa values of 35.2∼41.8 for water by applying the SSC(V)PE, which is greater than the experimental value of 15.7. In our calculation, the PCM also estimates greater pKa values than the experimental ones. Although the enthalpy and the entropy calculations are rather reliable, the solvation free energies are less reliable, because they come from the polarizations and/or reorientations of the solvent molecules from a microscopic point of view. A linear fit of calculated acid dissociation free energy difference, $\Delta G_{\text{solvent}}^{\mathbf{A}\to\mathbf{B}}$, to the experimental one, $\Delta G_{\text{solvent}}^{\mathbf{A}\to\mathbf{B}}(\text{exp.})$, gives the relational expression as

$$\Delta G_{\text{solvent}}^{\mathbf{A}\to\mathbf{B}}(\text{exp.}) = 0.66\Delta G_{\text{solvent}}^{\mathbf{A}\to\mathbf{B}} - 12.17 \tag{5}$$

where, $\Delta G_{\text{solvent}}^{\mathbf{A}\to\mathbf{B}}(\text{exp.})$ can be estimated by

$$\Delta G_{\text{solvent}}^{\mathbf{A}\to\mathbf{B}}(\text{exp.}) = 2.303RT \cdot \text{pKa}^{\text{exp}}. \tag{6}$$

The factor $2.303RT$ amounts to 1.4 kcal/mol at 300 K. Eq. 5 leads to a correlation coefficient of 0.996 and a slope of 0.66. If we assume that the discrepancies originate from the PCM solvation energies, the correction function on the PCM solvation energies is found to be

$$\Delta\Delta G_{\text{s,correct}}^{\mathbf{A}\to\mathbf{B}} = 0.9862\Delta\Delta G_{\text{s}}^{\mathbf{A}\to\mathbf{B}} - 25.77 \tag{7}$$

for the acid dissociation reaction. On the contrary, we can use the correction function for the acid association reaction as

$$\Delta\Delta G_{\text{s,correct}}^{\mathbf{A}\to\mathbf{B}} = 0.9862\Delta\Delta G_{\text{s}}^{\mathbf{A}\to\mathbf{B}} + 25.77 \tag{8}$$

The corrected pKa values, $\text{pKa}^{\text{correct}}$, using Eq. 7 are rather in good agreement with the experimental data. Therefore, the PCM model can reasonably reproduce the experimental pKa values for all calculated amino acids in water by taking the correction into consideration.

The general information on the solvation free energy can be easily derived by the Born model that considers the ion as a charged sphere immersed in a dielectric medium. The Born formula states that

$$\Delta G_{\text{s}}^{\text{Born}} = -\frac{z^2e^2}{8\pi\varepsilon_0 a}\left[\frac{1}{\varepsilon_{r,1}} - \frac{1}{\varepsilon_{r,2}}\right], \tag{9}$$

where ze is the charge of the ion, ε_0 is the permittivity of the vacuum state, a denotes the ionic radius, and $\varepsilon_{r,1}$ and $\varepsilon_{r,2}$ are the relative dielectric constants of states 1 and 2, respectively.

Table 3 Calculated thermodynamic properties concerning pKa for the proton acceptors compared with the experimental pKa values, pKa^{exp}, the free energy corrected pKa, $pKa^{correct}$, are also given

A/B	$\Delta H^{\mathbf{A}\to\mathbf{B}}$ (kcal/mol)	$-T\Delta S^{\mathbf{A}\to\mathbf{B}}$ (kcal/mol)	$\Delta\Delta G_s^{\mathbf{A}\to\mathbf{B}}$ (kcal/mol)	$\Delta G_{solvent}^{\mathbf{A}\to\mathbf{B}}$ (kcal/mol)	pKa^{calc}	$pKa^{correct}$	pKa^{exp}
$Asp + H_2O/Asp^- + H_3O^+$	168.5	−0.03	−144.0	24.5	17.5	0.5	3.3[a]
$Glu + H_2O/Glu^- + H_3O^+$	171.0	0.04	−144.3	26.7	19.1	2.1	4.1[a]
$HHis^+ + H_2O/His + H_3O^+$	74.1	−1.38	−39.6	33.1	23.7	5.7	6.8[a]
$Hdiglycine^+$/diglycine(enol)	74.9	−1.56	−34.2	39.2	28.0	9.9	9.1[b]
$HArg^+ + H_2O/Arg + H_3O^+$	78.3	1.61	−35.2	44.8	32.0	13.9	12.5[c]

[a] Ref. 19
[b] Ref. 20
[c] Ref. 21

For hydration, the usual quoted values for $\varepsilon_{r,1}$ and $\varepsilon_{r,2}$ are 1 (in vacuum) and 80 (in bulk water), respectively. Therefore the delocalization of charges corresponds to the increased radius a in Eq. 9 and leads to a low solvation energy.

Table 4 summarizes the thermodynamic properties concerning the free energy difference in the solvent, $\Delta G_{solvent}^{\mathbf{1}\to\mathbf{B}}$, along the reaction path for diglycine. The unfavorable formations of complexes **2** and **3**, ($\Delta G_{solvent}^{\mathbf{1}\to\mathbf{B}} > 0$), are interpreted as due to both the decrease in the entropy for complex formations and the unfavorable change in the aqueous solvation free energy, whereas a favorable contribution comes from the enthalpy stabilization ($\Delta H^{\mathbf{1}\to\mathbf{B}} < 0$). In general, the favorable change in the electronic energy is mostly compensated by the unfavorable electrostatics of solvation. For the Asp^- and Glu^- complexes, there exist two isolated ionic species of the oxonium cation and a proton acceptor anion in compound **1**, which show high solvation free energies. However, all molecules in complex **3** become charge neutral and the partial atomic charges are rather more delocalized over the complex than in the isolated state, thus the $\Delta\Delta G_s^{\mathbf{1}\to\mathbf{B}}$ increases. For the His and Arg complexes, the total net charges are kept throughout the proton transfer reaction, thus the positive solvation free energy changes $\Delta\Delta G_s^{\mathbf{1}\to\mathbf{B}}$ of ca. 50∼70 kcal/mol are considered to come from the charge delocalization in both complexes **2** and **3**. The entropy contributions for all complexes are close to each another due to the hydrogen bonding formations.

The free energy differences, $\Delta G_{solvent}^{\mathbf{1}\to\mathbf{B}}(\varepsilon = 80)$, of complex **3** depend on the pKa of the proton acceptor, and higher the pKa, the lower are the relative free energies. Applying the free energy correction on $\Delta\Delta G_{solvent}^{\mathbf{1}\to\mathbf{B}}$ ($\varepsilon = 80$) using Eq. 8 for the acid association reaction, the proton transfer reactions in model systems are concluded to be rare events in water. On the other hand, the relative dielectric constants surrounding the complexes become 2∼4 [10,18] in protein in contrast with 80 for bulk water. Therefore, proton transfer reaction though the peptide bond in protein becomes more favorable than in water, since the system will be enthalpy controlled in the protein. Indeed, $\Delta G_{solvent}^{\mathbf{1}\to\mathbf{B}}(\varepsilon = 4)$ becomes negative in complexes **2** and **3** for all proton acceptors. The free energy correction function in protein could not be obtained, since no experimental data was obtained. However, we have assumed that the dielectric constant used in the PCM calculation can describe free energy differences in protein, because the calculated hydration free energy differences using PCM model between a given pair of amino acids are well correlated with the experimental data. Thus, we have simply scaled the intercept of Eq. 8 by the factor of 0.75, which is roughly estimated as the ratio between $\Delta\Delta G_s^{\mathbf{1}\to\mathbf{B}}(\varepsilon = 4)$ and $\Delta\Delta G_s^{\mathbf{1}\to\mathbf{B}}(\varepsilon = 80)$. The corrected free energy differences, $\Delta G_{solvent}^{\mathbf{1}\to\mathbf{B}}(\varepsilon = 4)$, show that the proton transfer reactions are considered to be possible for Asp^-, Glu^-, and Arg complexes in protein. The corrected free energy of His complexes **2** and **3** are estimated to be 2.7 and 0.7 kcal/mol, respectively, and the activation free energy becomes 5.5 kcal/mol in this study. Thus, His complexes have two free energy minima along a proton transfer pathway. The double minimum of the free energy surface for the His complex in a protein may be used as the switch of the biological functions [29,30].

The solvation free energy change $\Delta\Delta G_s^{\mathbf{1}\to\mathbf{B}}$ in complex **3** is greater than that in complex **2** for His, in contrast to the Arg complex. These results can be accounted by the fact that the protonated $HHis^+$ in complex **3** is a kind of imidazorium cation, which makes resonance stabilization (scheme 1). Therefore, the solvation free energy $\Delta G_s^{HHis^+}$ becomes less negative. In addition, the proton release from the imidazorium cation makes δ- or ε-histidines. Our calculated thermodynamic properties for these tautomers are close to each other, in which $pKa^{correct}(\varepsilon = 80)$ becomes 4.6 and 5.7 for δ- and ε-His, respectively. Thus, we can consider that the double minimum for the His complex may assist the readily available tautomerization, as suggested by the biochemistry.

3.2 α-helix model

To elucidate the effects of the external electric field generated by the macrodipole of the α-helix on the proton transfer

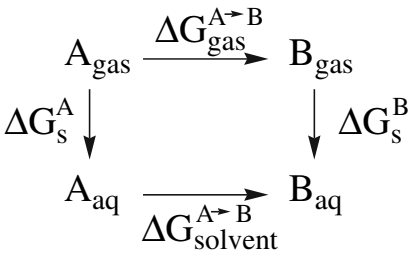

Thermodynamic Cycle 1

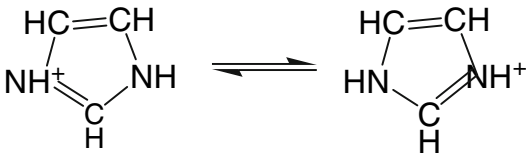

Scheme 1 SchemeI The resonating structure of imidazorium cation

reaction, the helix model that consists of the 12-mer polyglycine was applied. The calculated dipole moment of the helix model is 51.6 D in the vacuum state along the helix direction. In this subsection, only the Asp^- was used as the proton acceptor, which coordinated to the N-terminal glycine of the α-helix. The calculations were similar to those for the diglycine models described in sect. 3.1, except that diglycine was substituted by the 12-mer polyglycine helix. As optimizations require an enormous amount of computational effort to include the α-helix, the QM/MM methods were applied for optimizations using the B3LYP/6-31G+(d) level of theory, in which the structure in the MM region were fixed during optimizations. Then the PCM solvation energy calculations were applied for the optimized structures including the MM region. The relative dielectric constant was set to be 4 in the PCM calculations. Since it is impractical to carry out the frequency analysis due to our computer-resource limitations, the ZPE and entropy contributions were taken from the corresponding values listed in Table 4.

Table 5 summarizes the thermodynamic properties concerning the free energy differences in a solvent, $\Delta G^{\mathbf{1}\to\mathbf{B}}_{\text{solvent}}$, along the reaction pathway in the α-helix complexes, which was compared to the results of the diglycine models. The reaction is considered to be possible at the N-terminal domain in 12-mer helix, considering the correction. However, the calculated $\Delta G^{\mathbf{1}\to\mathbf{B}}_{c,\text{solvent}}$ of complex **3** is less favored in the helix than in the dipeptide model, where the unfavorable contributions consist of +5.2 kcal/mol in $\Delta\Delta G^{\mathbf{1}\to\mathbf{B}}_{\text{s}}$ and +7.6 kcal/mol in $\Delta H^{\mathbf{1}\to\mathbf{B}}$, in which $\Delta E^{\mathbf{1}\to\mathbf{B}} = +6.4$ kcal/mol. The former is accounted by the charge delocalization due to large molecular size of the α-helix complex. In order to clarify the reason why the energy destabilizations become significant in the helix models, the analysis of the intermolecular interaction energies, E_{int}, were carried out. E_{int} can be expanded as [7]

Table 4 Calculated thermodynamic properties concerning the free energy differences, $\Delta G^{\mathbf{1}\to\mathbf{B}}_{\text{solvent}}$, and the corrected free energy differences, $\Delta G^{\mathbf{1}\to\mathbf{B}}_{\text{c,solvent}}$, in the solvent (in kcal/mol)

	B	$\Delta H^{\mathbf{1}\to\mathbf{B}}$	$-T\Delta S^{\mathbf{1}\to\mathbf{B}}$	$\Delta\Delta G^{\mathbf{1}\to\mathbf{B}}_{\text{s}}$ ($\varepsilon=80$)	$\Delta\Delta G^{\mathbf{1}\to\mathbf{B}}_{\text{s}}$ ($\varepsilon=4$)	$\Delta G^{\mathbf{1}\to\mathbf{B}}_{\text{solvent}}$ ($\varepsilon=80$)	$\Delta G^{\mathbf{1}\to\mathbf{B}}_{\text{solvent}}$ ($\varepsilon=4$)	$\Delta G^{\mathbf{1}\to\mathbf{B}}_{\text{c,solvent}}$ ($\varepsilon=80$)	$\Delta G^{\mathbf{1}\to\mathbf{B}}_{\text{c,solvent}}$ ($\varepsilon=4$)
H_2O	**1**	0.0	0.0	0.0	0.0	0.0	0.0	0.0	0.0
	2	−79.5	19.6	59.7	44.2	−0.3	−15.7	24.7	3.0
	4	14.2	0.7	1.6	1.0	15.2	14.6	42.2	35.2
Asp^-	**1**	0.0	0.0	0.0	0.0	0.0	0.0	0.0	0.0
	3	−174.7	20.8	162.5	121.8	8.6	−32.1	32.1	−14.5
	4	−154.3	0.7	145.5	109.8	−8.0	−43.8	15.7	−26.0
Glu^-	**1**	0.0	0.0	0.0	0.0	0.0	0.0	0.0	0.0
	3	−175.6	20.7	162.4	121.9	7.5	−33.0	31.0	−15.3
	4	−156.8	0.7	145.9	110.2	−10.3	−45.9	13.5	−28.1
His	**1**	0.0	0.0	0.0	0.0	0.0	0.0	0.0	0.0
	2	−86.2	20.5	65.9	49.8	0.2	−15.9	25.0	2.7
	TS	−84.7	21.5	66.2	50.0	3.1	−13.2	27.9	5.5
	3	−93.3	22.2	71.9	53.2	0.8	−17.9	25.5	0.7
	4	−59.9	2.1	41.1	30.7	−16.7	−27.1	8.5	−8.2
Arg	**1**	0.0	0.0	0.0	0.0	0.0	0.0	0.0	0.0
	2	−92.6	21.3	66.6	52.4	−4.7	−18.9	20.1	−0.4
	TS	−93.8	22.1	66.7	52.3	−5.0	−19.4	19.8	−0.8
	3	−98.3	20.5	64.6	51.1	−13.1	−26.6	11.7	−8.1
	4	−64.1	−0.9	37.5	27.6	−27.5	−37.4	−2.3	−18.5

Table 5 Calculated thermodynamic properties concerning the free energy differences, $\Delta G^{\mathbf{1}\to\mathbf{B}}_{\text{solvent}}$, and the corrected free energy differences, $\Delta G^{\mathbf{1}\to\mathbf{B}}_{\text{c,solvent}}$, in the protein (in kcal/mol)

		Electronic energy (hartree)	$\Delta H^{\mathbf{1}\to\mathbf{B}}$ (kcal/mol)	$-T\Delta S^{\mathbf{1}\to\mathbf{B}}$ (kcal/mol)	$\Delta\Delta G^{\mathbf{1}\to\mathbf{B}}_{\text{s}}$ (kcal/mol)	$\Delta G^{\mathbf{1}\to\mathbf{B}}_{\text{solvent}}$ (kcal/mol)	$\Delta G^{\mathbf{1}\to\mathbf{B}}_{\text{c,solvent}}$ (kcal/mol)
Diglycine	**1**	−930.43731	0.0	0.0	0.0	0.0	0.0
	3	−930.72002	−174.7	20.8	121.8	−32.1	−14.5
	4	−930.68344	−154.3	0.7	109.8	−43.8	−26.0
12mer	**1**	−3085.82843	0.0	0.0	0.0	0.0	0.0
	3	−3086.10099	−167.1	20.8	127.0	−19.4	−1.8
	4	−3086.06825	−150.3	0.7	109.6	−40.0	−22.2

$$E_{\text{int}} = \sum_i \Delta E^{(1)}[i] + \sum_{i>j} \Delta E^{(2)}[i:j] + \sum_{i>j} \Delta E^{(2)}[i:j] + \sum_{i>j>k} \Delta E^{(3)}[i:j:k] + \cdots, \tag{10}$$

$$\Delta E^{(1)}[i] = E^{\text{comp}}[i] - E^{\text{opt}}[i], \tag{11}$$

$$\Delta E^{(2)}[i:j] = E^{\text{comp}}[i:j] - E^{\text{comp}}[i] - E^{\text{comp}}[j], \tag{12}$$

$$\Delta E^{(3)}[i:j:k] = E^{\text{comp}}[i:j:k] - \sum_{l\in i,j,k} E^{\text{comp}}[l] - \sum_{\substack{l>m \\ l,m\in i,j,k}} \Delta E^{(2)}[l:m], \tag{13}$$

where $\Delta E^{(1)}[i]$ is the deformation energy of the molecule i. $\Delta E^{\text{opt}}[i]$ is the energy of an isolated optimized structure of the molecule i, and $\Delta E^{\text{comp}}[i:j:k:\cdots]$ is the energies of the molecular subgroups consisting of molecules $i, j, k, \ldots$, which are members of the given complex. In these expressions, $\Delta E^{(2)}[i:j]$ and $\Delta E^{(3)}[i:j:k]$ are called the two- and three-body interaction energies, respectively.

For the purpose of describing the effects of the dipole moment on the intermolecular interactions, we will additionally define the following notations:

$$\Delta\Delta E^{(1)}_{\mathbf{B}}[i] = \left\{\Delta E^{(1)}_{\mathbf{B}}[i] - \Delta E^{(1)}_{\mathbf{1}}[i]\right\}_{\text{helix}} - \left\{\Delta E^{(1)}_{\mathbf{B}}[i] - \Delta E^{(1)}_{\mathbf{1}}[i]\right\}_{\text{diglycine}}, \tag{14}$$

$$\Delta\Delta E^{(2)}_{\mathbf{B}}[i,j] = \left\{\Delta E^{(2)}_{\mathbf{B}}[i,j] - \Delta E^{(2)}_{\mathbf{1}}[i,j]\right\}_{\text{helix}} - \left\{\Delta E^{(2)}_{\mathbf{B}}[i,j] - \Delta E^{(2)}_{\mathbf{1}}[i,j]\right\}_{\text{diglycine}}, \tag{15}$$

etc., where $\Delta E^{(1)}_{\mathbf{B}}[i]$ is the deformation energy $\Delta E^{(1)}[i]$ in complex **B**. Then, $\Delta\Delta E^{(1)}_{\mathbf{B}}[i]$ represents the stabilization (negative) or destabilization (positive) energies of the deformation energy affected by the macrodipole moment of the α-helix. In the same way, $\Delta\Delta E^{(2)}_{\mathbf{B}}[i,j]$ is for two-body interactions. Since complex **3** is the only avaliable energy minimum structure in Asp^-, we have focused attension on complex **3**.

Table 6 Component analysis of intermolecular interaction energies for the α-helix complex **3**. Stabilization energies of deformation $\Delta\Delta E^{(1)}_{\mathbf{3}}$, two body $\Delta\Delta E^{(2)}_{\mathbf{3}}$, and three body interactions $\Delta\Delta E^{(3)}_{\mathbf{3}}$ affected by the dipole moment of the α-helix (in kcal/mol)

i	$\Delta\Delta E^{(1)}_{\mathbf{3}}$	$i:j$	$\Delta\Delta E^{(2)}_{\mathbf{3}}$	$i:j:$k	$\Delta\Delta E^{(3)}_{\mathbf{3}}$
Asp	1.2	Asp:H_2O	−0.2	Asp:Helix:H_2O	−0.9
H_2O	−0.5	Asp:Helix	−1.6		
Helix	5.9	Helix:H_2O	2.7		

The component analysis in Table 6 shows that the helix dipole moment destabilizes 5.9 kcal/mol on the helical alignment of the polyglycine chain in complex **3** due to the charge–dipole repulsive interactions between the N-terminal domain and the helix dipole moment. Additionally, despite the favorable interactions of −1.6 kcal/mol between Asp and the helix dipole, the unfavorable interaction between the H_2O molecule and the helix dipole of 2.7 kcal/mol overcomes this stabilization. The accumulated energy listed in Table 6 is +6.4 kcal/mol which can reproduce $\Delta E^{\mathbf{1}\to\mathbf{B}}$ in complex **3**. The α-helix is estimated to suppress the proton transfer reactions through the peptide bond at the termini of the α-helix, although it is possible to proceed when the proton affinity of the acceptor is low.

4 Conclusion

We have investigated the systematic environmental effects on the proton transfer reaction through the peptide bond using both diglycine and 12-mer polyglycine α-helix models. The solvation effects were taken into consideration by applying PCM with the Merz–Kollman cavity under the B3LYP/6-31+G(d) level of theory. We could find the correction functions on the calculated solvation energies for the acid dissociation reaction. The corrected free energy changes could reasonably reproduce the experimental pKa values for all amino acids considered in this paper.

In the diglycine model, the proton transfer reactions in model systems are concluded to be rare events in water. However, it becomes possible for Asp^-, Glu^- and Arg complexes in the protein represented by low relative dielectric constant. We have found that His complex has two free energy minima along a proton transfer pathway in spite of one minimum in the other complexes. The double minimum of the free energy surface for the His complex in a protein may be used as the switch of the biological functions.

The α-helix tends to suppress the proton transfer reaction through the peptide bond at the terminal of the helix, although it is possible to proceed when the PA of the acceptor is low. The unfavorable contributions in the α-helix come from both the charge delocalizations and the charge–dipole interactions.

Acknowledgments This work was supported by the Next Generation Super Computer Project, Nanoscience Program, MEXT, Japan. The first author acknowledges with sincere appreciation the financial support provided by the Core Research for Evolutional Science and Technology (CREST) "High Performance Computing for Multi-scale and Multi-physics Phenomena" of the Japan Science and Technology Agency. A part of this work was supported by the Nanotechnology Support Project of the Ministry of Education, Culture, Sports, Science and Technology (MEXT), Japan.

References

1. Asada T, Haraguchi H, Kitaura K (2001) J Phys Chem A 105:7423
2. Cazar R, Jamka A, Tao F (1998) Chem Phys Lett 287:549
3. Cazar R, Jamka A, Tao F (1998) J Phys Chem 102:5117
4. Jaroszewski L, Lesyng B, McCammon JA (1993) J Mol Struct (Theochem) 283:57
5. Li G, Martines C, Marilia TC, Millot C, Ruiz-Lopez MF (1999) Chem Phys 240:93
6. Snyder JA, Cazar RA, Jamka AJ, Tao F (1999) J Phys Chem A 103:7719
7. Asada T, Takitani S, Koseki S (2005) J Phys Chem A 109:1821
8. Komatsuzaki T, Iwao O (1996) Mol Simul 16:321
9. Lapid H, Agmon N, Petersen MK, Voth GA (2005) J Chem Phys 122:14506
10. Takano Y, Nakamura H (2006) Chem Phys Lett 430:149
11. Tsukihara T, Shimokata K, Katayama Y, Shimada H, Muramoto K, Aoyama H, Mochizuki M, Shinzawa-Itoh K, Tsukihara T, Shimokata K, Katayama Y, Shimada H, Muramoto K, Aoyama H, Mochizuki M, Shinzawa-Itoh K, Yamashita E, Yao M, Ishimura Y, Yoshikawa S (2003) PNAS 100:15304
12. Miertus S, Scrocco E, Tomasi J (1981) Chem Phys 55:117
13. Meyer H D (1986) J Chem Phys 84:3147
14. Mezei M, Beveridge DL (1981) J Chem Phys 74:6902
15. Joshi HV, Meier M (1996) J Am Chem Soc 118:12038
16. Miller JS, Kennedy RJ, Kemp DS (2002) J Am Chem Soc 124:945
17. Sek S, Swiatek K, Misicha A (2005) J Phys Chem B 109:23121
18. Sengupta D, Behera RN, Smith JC, Ullmann GM (2005) Structure 13:849
19. Richarz R, Wuthrich K (1975) Biopolymers 17:2133
20. Matthew JB, Gurd FRN, Garcia-Moreno B, Flanagan MA, March KL, Shire SJ (1985) CRC Cri Rev Biochem 18:91
21. Pine SH, Hendrickson JB, Cram DJ, Hammond GS (1980) organic chemistry, 4th edn. McGraw-Hill, New York
22. Frisch MJ, Trucks GW, Schlegel HB, Scuseria GE, Robb MA, Cheeseman JR, Montgomery JA Jr, Vreven T, Kudin KN, Burant JC, Millam JM, Iyengar SS, Tomasi J, Barone V, Mennucci B, Cossi M, Scalmani G, Rega N, Petersson GA, Nakatsuji H, Hada M, Ehara M, Toyota K, Fukuda R, Hasegawa J, Ishida M, Nakajima T, Honda Y, Kitao O, Nakai H, Klene M, Li X, Knox JE, Hratchian HP, Cross JB, Bakken V, Adamo C, Jaramillo J, Gomperts R, Stratmann RE, Yazyev O, Austin AJ, Cammi R, Pomelli C, Ochterski JW, Ayala PY, Morokuma K, Voth GA, Salvador P, Dannenberg JJ, Zakrzewski VG, Dapprich S, Daniels AD, Strain MC, Farkas O, Malick DK, Rabuck AD, Raghavachari K, Foresman JB, Ortiz JV, Cui Q, Baboul AG, Clifford S, Cioslowski J, Stefanov BB, Liu G, Liashenko A, Piskorz P, Komaromi I, Martin RL, Fox DJ (2004) Gaussian, Inc., Wallingford CT
23. Chase MW Jr (1998) NIST-JANAF thermochemical tables, 4th edn. J Phys Chem Ref Data Monogr 9:1–195
24. Bojesan G, Breindahl T (1994) J Phys Chem Soc Perkin Trans 2:1029
25. Hunter EPL, Lias SG (1998) J Chem Ref Data 27:413
26. Janusz R, Piotr S, Jack S, Maciej G (2001) J Am Chem Soc 123:11695
27. Wang J, Cieplak P, Kollman PA (2000) J Comp Chem 21:1049
28. Chipman DM. (2002) J Phys Chem A 106:7413
29. Wolff N, Deniau C, Letoffe S, Simenel C, Kumar V, Stojiljkovic I, Wandersman C, Delephierre M, Lecroisey A (2002) Protein Sci 11:757
30. Todt JC, McGroarty EJ (1992) Biochemistry 31:10479